Vit Dolejsi and Miloslav Feistauer

On the Discontinuous Galerkin Method for the Numerical Solution of Compressible High-Speed Flow

Preprint No. MATH-knm-2002/1

07.01.2002

Submitted to *Proceeding of ENUMATH'01 conference*

Department of Numerical Mathematics, Faculty of Mathematics and Physics, Charles University, Sokolovská 83, 186 75 Praha 8, Czech Republic

http://www.karlin.mff.cuni.cz/ms-preprints/

Cover print by Reprostředisko, Malostranské nám. 25, Praha 1 - Malá Strana
Design by Mirko Rokyta, picture of snowflake by Ondřej Kalenda
Current series administrator: V. Dolejsi

On the Discontinuous Galerkin Method for the Numerical Solution of Compressible High-Speed Flow

Vít Dolejší and Miloslav Feistauer

Faculty of Mathematics and Physics, Charles University Prague, Czech Republic
dolejsi@karlin.mff.cuni.cz, feist@karlin.mff.cuni.cz

Summary. The paper deals with an application of the discontinuous Galerkin finite element (DG FE) method to the numerical solution of the system of hyperbolic equations. We extend our results from [8], [9], where two versions of the DG FE method were applied to the scalar convection–diffusion equation. In order to avoid spurious oscillations near discontinuities we develop a new limiting which is based on the control of interelement jumps and switches from piecewise linear to piecewise constant approximations. Isoparametric finite elements are used near a curved boundary of nonpolygonal computational domain in order to achieve a physically admissible and sufficiently accurate numerical solution. Numerical examples of transonic flow through the GAMM channel and around the NACA0012 airfoil are presented. Finally, we mention some theoretical results obtained for a modified DG FE method applied to a nonlinear convection-diffusion problem.

1 Introduction

Our goal is to develop a sufficiently accurate and robust method for the numerical solution of nonlinear conservation laws, nonlinear convection-diffusion problems and compressible flow. During last years we developed combined finite volume (FV) – finite element (FE) methods which give good results in many cases of technically relevant problems in complex domains. For analysis and applications, see, e. g., [1], [11], [12], [13], [14], [15]. However, their drawback is the necessity to construct two mutually associated meshes, which is rather complicated particularly in 3D ([16]) and, moreover, the schemes suffer from a high amount of numerical viscosity as FV – FE methods are only of the first order of accuracy.

A generalization of FV and FE methods is the discontinuous Galerkin finite element (DG FE) method based on piecewise polynomial approximations without any requirement of the interelement continuity. It uses only one mesh and allows higher order of accuracy. Recently, the DG FE method has become quite popular and is discussed in a number of papers. For a survey about DG FE methods, see, [5] or [6]. Let us mention particularly the works [2] and [3] concerned with subsonic compressible flow and papers [4] and [20] on theoretical analysis of this method applied to linear problems.

Various numerical experiments indicate that the DG FE method is particularly suitable for the numerical solution of nonlinear conservation laws with discontinuous solutions and nonlinear convection-diffusion problems whose solutions have steep gradients. This is the subject of this paper. Our goal is to develop sufficiently accurate schemes for nonlinear conservation laws and convection-diffusion problems which produce numerical solutions not suffering from the so-called spurious oscillations in the vicinity of discontinuities and steep gradients. The main applications are oriented to the simulation of compressible high-speed flow.

In order to avoid spurious oscillations, we propose a suitable limiting of the order of accuracy of the method based on a local averaging procedure. In [8] and [9] we developed two methods for scalar nonlinear convection-diffusion problems and conservation laws. Here our main emphasis is put on the application to the Euler equations describing inviscid gas flow.

In Section 2 we introduce the formulation of the continuous problem. Section 3 is concerned with the definition of the DG FE solution. In Section 4 we extend the limiting from [9] to the system of the Euler equations. A special attention is paid to problems in nonpolygonal computational domains. Numerical experiments show that it is necessary to use isoparametric finite elements in order to obtain a good resolution near a curved part of the boundary, see Section 5. Numerical examples are in Section 6. Finally, we present some results of theoretical analysis of the problem.

2 Governing equations

In a space-time cylinder $Q_T = \Omega \times (0,T)$ we consider the first order hyperbolic system

$$\frac{\partial \boldsymbol{w}}{\partial t} + \sum_{s=1}^{2} \frac{\partial \boldsymbol{f}_s(\boldsymbol{w})}{\partial x_s} = 0 \tag{1}$$

describing inviscid compressible flow in a plane bounded domain Ω and time interval $(0,T)$. Here

$$\boldsymbol{w} = (\rho,\, \rho v_1,\, \rho v_2,\, e)^{\mathrm{T}}, \quad \boldsymbol{w} = \boldsymbol{w}(\boldsymbol{x},t), \quad \boldsymbol{x} \in \Omega, \quad t \in (0,T),$$
$$\boldsymbol{f}_s(\boldsymbol{w}) = (\rho v_s,\, \rho v_s v_1 + \delta_{s1} p,\, \rho v_s v_2 + \delta_{s2} p,\, (e+p)\, v_s)^{\mathrm{T}}, \ s = 1,2$$

and p is given by the state equation

$$p = (\gamma - 1)\,(e - \rho|\boldsymbol{v}|^2/2). \tag{2}$$

We use the standard notation: t – time, $\boldsymbol{x} = (x_1, x_2)$ – Cartesian coordinates, ρ – density, p – pressure, e – total energy, $\boldsymbol{v} = (v_1, v_2)$ – velocity, δ_{ij} – Kronecker delta, $\gamma > 1$ is the Poisson adiabatic constant.

The system (1) – (2) is equipped with the initial condition

$$\boldsymbol{w}(\boldsymbol{x},0) = \boldsymbol{w}^0(\boldsymbol{x}) \quad \forall \boldsymbol{x} \in \Omega, \tag{3}$$

where $\boldsymbol{w}^0$ is a given function, and a set of boundary conditions. For their description see, e. g., [10].

3 Discretization

3.1 Broken Sobolev space

In what follows we use the standard notation for function spaces: $H^k(\Omega) =$ Sobolev space, $L^2(0,T;X) =$ Bochner space of square integrable functions on $(0,T)$ with values in a Banach space X, $C^1(0,T;X) =$ space of continuously differentiable mappings in $(0,T)$ with values in X.

Let Ω_h be a polygonal approximation of Ω. In order to derive the discrete problem, we consider a mesh $\mathcal{T}_h$ of Ω_h consisting of various types of convex elements $K_i \in \mathcal{T}_h,\ i \in I$ ($I =$ a suitable index set), e. g., triangles, quadrilaterals, polygons, or their combinations.

By Γ_{ij} we denote a common edge between two neighbouring elements K_i and K_j. The symbol $\boldsymbol{n}_{ij} = ((n_{ij})_1, (n_{ij})_2)$ denotes the unit outer normal to ∂K_i on the side Γ_{ij}. Moreover, we denote the set of all neighbours of K_i by $s(i) = \{j \in I; K_j$ is a neighbour of $K_i\}$. The boundary $\partial\Omega_h$ is formed by a finite number of faces of elements K_i adjacent to $\partial\Omega_h$. We denote all these boundary faces by S_j, where $j \in I_b \subset Z^- = \{-1,-2,\ldots\}$. We set $\gamma(i) = \{j \in I_b; S_j$ is a face of $K_i\}$ and $\Gamma_{ij} = S_j$ for $K_i \in \mathcal{T}_h$ such that $S_j \subset \partial K_i,\ j \in I_b$. For K_i not containing any boundary face S_j we set $\gamma(i) = \emptyset$. Obviously, $s(i) \cap \gamma(i) = \emptyset$ for all $i \in I$. Now, if we write $S(i) = s(i) \cup \gamma(i)$, we have

$$\partial K_i = \bigcup_{j \in S(i)} \Gamma_{ij}. \tag{4}$$

We define the so-called *broken Sobolev space*

$$H^k(\Omega, \mathcal{T}_h) = \{v; v|_K \in H^k(K)\ \forall\, K \in \mathcal{T}_h\}. \tag{5}$$

In order to derive the discrete problem, we multiply (1) by a function $\boldsymbol{\varphi} \in \left[H^k(\Omega, \mathcal{T}_h)\right]^4$ and integrate over an element $K_i,\ i \in I$. With the use of Greens theorem, we obtain the integral identity

$$\begin{aligned}\frac{\partial}{\partial t}\int_{K_i} \boldsymbol{w}\cdot\boldsymbol{\varphi}\,\mathrm{d}\boldsymbol{x} &= \int_{K_i}\sum_{s=1}^{2}\boldsymbol{f}_s(\boldsymbol{w})\cdot\frac{\partial\boldsymbol{\varphi}}{\partial x_s}\,\mathrm{d}\boldsymbol{x} \\ &- \sum_{j\in S(i)}\int_{\Gamma_{ij}}\sum_{s=1}^{2}\boldsymbol{f}_s(\boldsymbol{w})\cdot\boldsymbol{\varphi}\,n_s\,\mathrm{d}S,\end{aligned} \tag{6}$$

where $\boldsymbol{n}_{ij} = (n_1, n_2)$ is the unit outer normal to element K_i. Summing (6) over all $K_i \in \mathcal{T}_h$, we obtain the identity

$$\begin{aligned}\frac{\partial}{\partial t}\sum_{K_i\in\mathcal{T}_h}\int_{K_i}\boldsymbol{w}\cdot\boldsymbol{\varphi}\,\mathrm{d}x &= \sum_{K_i\in\mathcal{T}_h}\int_{K_i}\sum_{s=1}^{2}\boldsymbol{f}_s(\boldsymbol{w})\cdot\frac{\partial\boldsymbol{\varphi}}{\partial x_s}\,\mathrm{d}x - \\ &- \sum_{K_i\in\mathcal{T}_h}\sum_{j\in S(i)}\int_{\Gamma_{ij}}\sum_{s=1}^{2}\boldsymbol{f}_s(\boldsymbol{w})\cdot\boldsymbol{\varphi}\,n_s\,\mathrm{d}S.\end{aligned} \tag{7}$$

This equality represents a weak form of the Euler equations in the sense of the broken Sobolev space $H^1(\Omega, \mathcal{T}_h)$.

3.2 Numerical solution

Now we shall introduce the discrete problem approximating identity (7) – (8) with the aid of the discontinuous Galerkin method. To evaluate the boundary integral in (7) we use the approximation

$$\int_{\Gamma_{ij}} \sum_{s=1}^{2} \boldsymbol{f}_s(\boldsymbol{w}(t))\, n_s \cdot \boldsymbol{\varphi}\, \mathrm{d}S \approx \int_{\Gamma_{ij}} \boldsymbol{H}(\boldsymbol{w}^+(\boldsymbol{x},t), \boldsymbol{w}^-(\boldsymbol{x},t), \boldsymbol{n}_{ij}) \cdot \boldsymbol{\varphi}(\boldsymbol{x}) \mathrm{d}S, \quad (8)$$

where $\boldsymbol{H}$ is *the numerical flux*, $\boldsymbol{w}^+(\boldsymbol{x},\cdot)$ and $\boldsymbol{w}^-(\boldsymbol{x},\cdot)$ are the values of $\boldsymbol{w}$ at $\boldsymbol{x} \in \Gamma_{ij}$ considered from interior and exterior of K_i, respectively. For evaluation of $\boldsymbol{H}$ we use the Osher–Solomon numerical flux, see [19, 21, 17].

We define the space of discontinuous piecewise polynomial functions

$$S_h \equiv S^{p,-1}(\Omega, \mathcal{T}_h) = \{v; v|_K \in P_p(K)\ \forall\, K \in \mathcal{T}_h\}, \quad (9)$$

where $P_p(K)$ denotes the space of all polynomials on K of degree $\leq p$. Moreover, for $\boldsymbol{w}_h, \boldsymbol{\varphi}_h \in S_h$ we introduce the forms

$$\begin{aligned}
(\boldsymbol{w}_h, \boldsymbol{\varphi}_h) &= \int_{\Omega} \boldsymbol{w}_h(\boldsymbol{x},t) \cdot \boldsymbol{\varphi}_h(\boldsymbol{x})\, \mathrm{d}\boldsymbol{x}, \\
b_h(\boldsymbol{w}_h, \boldsymbol{\varphi}_h) &= -\sum_{K \in \mathcal{T}_h} \int_K \sum_{s=1}^{2} \boldsymbol{f}_s(\boldsymbol{w}_h(\boldsymbol{x},t)) \cdot \frac{\partial \boldsymbol{\varphi}_h(\boldsymbol{x})}{\partial x_s}\, \mathrm{d}\boldsymbol{x} \qquad (10) \\
&\quad + \sum_{K_i \in \mathcal{T}_h} \sum_{j \in S(i)} \int_{\Gamma_{ij}} \boldsymbol{H}(\boldsymbol{w}_h^+(\boldsymbol{x},t), \boldsymbol{w}_h^-(\boldsymbol{x},t), \boldsymbol{n}_{ij}) \cdot \boldsymbol{\varphi}_h(\boldsymbol{x}) \mathrm{d}S
\end{aligned}$$

and we say that $\boldsymbol{w}_h$ is the *approximate solution* of (1) if satisfies the conditions

$$\begin{aligned}
&\text{a)}\ \ \boldsymbol{w}_h \in C^1([0,T], [S_h]^4), \\
&\text{b)}\ \ \frac{\partial}{\partial t}(\boldsymbol{w}_h(t), \boldsymbol{\varphi}_h) + b_h(\boldsymbol{w}_h(t), \boldsymbol{\varphi}_h) = 0 \qquad \forall\, \boldsymbol{\varphi}_h \in [S_h]^4\ \forall\, t \in (0,T), \quad (11) \\
&\text{c)}\ \ \boldsymbol{w}_h(0) = \boldsymbol{w}_h^0.
\end{aligned}$$

Relations (11) represent a system of ordinary differential equations which can be solved by a suitable numerical method.

3.3 Implementation

The computation of the approximate solution was realized over regular triangular grids with the aid of piecewise linear approximations, i. e., with $p = 1$ in

(9). We use the basis of $S_h := S^{1,-1}$ whose components are piecewise linear functions associated with midpoints of sides of triangles:

$$\{\phi_{ij} \in S_h; \phi_{ij}(Q_{kl}) = \delta_{ik}\delta_{jl},\ j \in S(i), l \in S(k), i,k \in I\}, \tag{12}$$

where Q_{kl} is the midpoint of Γ_{kl}. This choice leads to a diagonal mass matrix in (11,b). In (8) we use the two point Gauss quadrature rule

$$\int_{-1}^{1} g(t)\,\mathrm{d}t \approx g\left(-\frac{1}{\sqrt{3}}\right) + g\left(\frac{1}{\sqrt{3}}\right) \tag{13}$$

which is exact for polynomials of the third degree and the volume integrals in (6) are evaluated by the three point integration rule

$$\int_{K_i} g(\boldsymbol{x})\,\mathrm{d}\boldsymbol{x} \approx \frac{1}{3} \sum_{j \in S(i)} g(Q_{ij}), \tag{14}$$

which is exact for second degree polynomials. The system of ordinary differential equations (11) is solved by the forward Euler method. It is necessary to use a suitable stability condition of the form $\Delta t = O(h)$. Numerical experiments show that the scheme has a second order of accuracy in space provided that the exact solution is sufficiently regular.

Our method can be considered as an extension of the finite volume method, which uses piecewise constant approximations, i.e., $p = 0$ in (9).

4 Limiting

Nonlinear hyperbolic equations have often discontinuous exact solutions. Their numerical approximations obtained by (11) usually contain overshoots, undershoots and spurious oscillations. In order to avoid these unphysical phenomena, we developed an indicator which seeks elements $K \in \mathcal{T}_h$ on which the approximate solution has large interelement jumps, representing discontinuities. On these elements the order limiting is applied, switching from a piecewise linear approximation to a piecewise constant approximation.

Numerical experiments carried out in [9] for scalar conservation laws show that the interelement jumps in the approximate solution are of the order $O(1)$ on discontinuities, whereas $O(h^2)$ in the areas where the solution is regular. Therefore, the interelement jumps of order $O(h^\alpha)$ with $\alpha \in (0,2)$ represent a natural interface between "smooth" and "discontinuous" parts of the solution. In [9] we showed that for the case of a scalar equation, it is suitable to measure the magnitude of interelement jumps of the numerical solution u_h in the integral form by

$$\int_{\partial K_i} [\![u_h]\!]^2\,\mathrm{d}S, \quad K_i \in \mathcal{T}_h, \tag{15}$$

where $[\![u_h]\!]$ denotes the jump of u_h on sides of K_i.

Here we extend the control of jumps also for the system of the Euler equations (1). In order to detect discontinuities of the solutions (shock waves, contact discontinuities), it is suitable to measure the jumps of the density. Based on presented results and numerical experiments we define the *jump indicator*

$$g(i) = \frac{\int_{\partial K_i} ([\![\rho]\!])^2 \, \mathrm{d}S}{h_i |K_i|^{3/4}}, \tag{16}$$

which is of order $O(1)$, if $[\![\rho]\!] = O(h^{3/4})$.

Now, for each time step we apply the limitation procedure which modifies the approximate solution $\boldsymbol{w}_h$ in the following way:

$$\boldsymbol{w}_h|_{K_i} := \begin{cases} \bar{\boldsymbol{w}}_h|_{K_i} & \text{if } g(i) > 1, \\ \boldsymbol{w}_h|_{K_i} & \text{otherwise,} \end{cases} \quad K_i \in \mathcal{T}_h, \tag{17}$$

where

$$\bar{\boldsymbol{w}}_h|_{K_i} \in P_0(K_i), \ \bar{\boldsymbol{w}}_h|_{K_i} = \frac{1}{K_i} \int_{K_i} \boldsymbol{w}_h \, \mathrm{d}\boldsymbol{x}. \tag{18}$$

Numerical examples confirm a high efficiency of the limiting procedure (16) – (18). Namely, Figures 5 and 7 show the capturing of the discontinuity (shock wave) without any unphysical oscillation.

5 Isoparametric elements at a curved boundary

Numerical experiments show that in some cases the DG FE method does not give good resolution in a neighbourhood of curved parts of the boundary $\partial\Omega$. In order to get a good quality solution, it is necessary to use isoparametric finite elements or a suitable numerical integration, see [2] and [18].

Let $\{K_i, \ i \in I_c, \ I_c \subset I\}$ be a set of triangles adjacent to a curved part of $\partial\Omega$, see Figure 1. Let $P_i^k, \ k = 0, 1, 2$ be the vertices of K_i and moreover $P_i^k \in \partial\Omega$ for $k = 1, 2$ and $i \in I_c$. We suppose that the centre $P_i^{12} \in \partial\Omega$ of the curved side with endpoints P_i^1, P_i^2 is close to the centre of the straight segment $P_i^1 P_i^2$. See Figure 1.

Then there exists a unique *bilinear* mapping $F_i : \hat{K} \to K_i, F_i = (F_i^1, F_i^2)$ such that

$$\begin{aligned} F_i(\hat{P}^k) &= P_i^k, \quad k = 0, 1, 2, \\ F_i(\hat{P}^{12}) &= P_i^{12}, \end{aligned} \tag{19}$$

where $\hat{K}$ is a reference triangle with vertices

$$\hat{P}^0 = [0; 0], \quad \hat{P}^1 = [1; 0], \quad \hat{P}^2 = [0; 1] \tag{20}$$

and

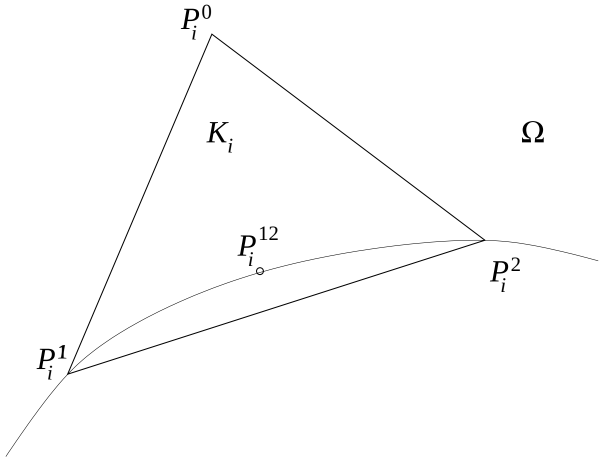

Fig. 1. Triangle K_i lying on a curved part of $\partial\Omega$

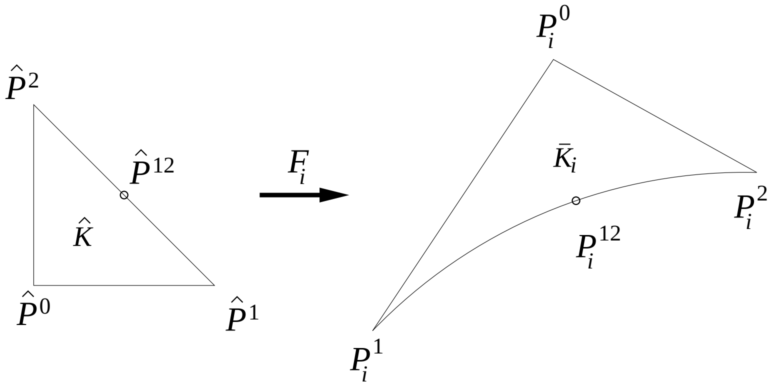

Fig. 2. Bilinear mapping $F_i : \hat{K} \to K_i$

$$\hat{P}^{12} = [1/2; 1/2], \tag{21}$$

see Figure 2.

Then triangles $K_i,\ i \in I_c$ are replaced by the curved triangles defined by

$$\bar{K}_i = F_i(\hat{K}). \tag{22}$$

The set $\bar{K}_i$ is a plane figure having two straight sides and one curved side, see Figure 2. If $i \notin I_c$ then F_i is a linear mapping and, therefore, $\bar{K}_i = K_i$.

Now let us describe how to evaluate the volume and boundary integrals over elements $\bar{K}_i,\ i \in I_c$ and their sides Γ_{ij}. We denote by

$$J_{F_i}(\hat{\boldsymbol{x}}) \equiv \frac{D\,F_i}{D\,\hat{\boldsymbol{x}}}(\hat{\boldsymbol{x}}), \quad \hat{\boldsymbol{x}} \in \hat{K}, \tag{23}$$

the Jacobi matrix of the mapping F_i. Since F_i is bilinear, we easily find out that $\det J_{F_i}$ is a linear function of the variable $\hat{\boldsymbol{x}}$. The components of the vector valued test functions $\boldsymbol{\varphi}_h$ from (11) are defined on the boundary elements $\bar{K}_i$ with the aid of the mapping F_i. Denoting by $\hat{\varphi}$ any linear function on the reference element $\hat{K}$, we set

$$\varphi_h(\boldsymbol{x}) = \hat{\varphi}(F_i^{-1}(\boldsymbol{x})), \quad \boldsymbol{x} \in K_i. \tag{24}$$

These functions form the components of the test functions from the discrete problem. Then the integrals in (10) are evaluated in the following way:

The first form in (10) is expressed as

$$\int_{\bar{K}_i} \boldsymbol{w}_h(\boldsymbol{x}, t) \cdot \boldsymbol{\varphi}_h(\boldsymbol{x}) \, \mathrm{d}\boldsymbol{x} = \int_{\hat{K}} \det J_{F_i}(\hat{\boldsymbol{x}}) \hat{\boldsymbol{w}}_i(\hat{\boldsymbol{x}}, t) \cdot \boldsymbol{\varphi}_h(\hat{\boldsymbol{x}}) \, \mathrm{d}\hat{\boldsymbol{x}}, \quad i \in I, \tag{25}$$

where $\hat{\boldsymbol{w}}_i(\hat{\boldsymbol{x}}, t) = \boldsymbol{w}_h(F_i^{-1}(\boldsymbol{x}), t)$.

Moreover, the volume integral in the form b_h in (10) is computed with the aid of

$$\begin{aligned} &\int_{\bar{K}_i} \sum_{s=1}^{2} \boldsymbol{f}_s(\boldsymbol{w}_h(\boldsymbol{x}, t)) \cdot \frac{\partial \boldsymbol{\varphi}_h(\boldsymbol{x})}{\partial x_s} \, \mathrm{d}\boldsymbol{x} \\ &= \int_{\hat{K}} \det J_{F_i}(\hat{\boldsymbol{x}}) \sum_{s=1}^{2} \boldsymbol{f}_s(\hat{\boldsymbol{w}}_i(\hat{\boldsymbol{x}}, t)) \cdot \sum_{j=1}^{2} \frac{\partial \hat{\boldsymbol{\varphi}}}{\partial \hat{x}_j} \frac{\partial (F_i^{-1})^j(F_i(\hat{\boldsymbol{x}}))}{\partial x_s} \, \mathrm{d}\hat{\boldsymbol{x}}, \quad i \in I, \end{aligned} \tag{26}$$

where $(F_i^{-1})^j$ denotes the j-th component of the inverse mapping F_i^{-1}. In order to compute the inverse mapping F_i^{-1} we use the following relation written in the matrix form:

$$\frac{D\,F_i^{-1}}{D\boldsymbol{x}}(F_i(\hat{\boldsymbol{x}})) = \left[\frac{D\,F_i}{D\hat{\boldsymbol{x}}}(\hat{\boldsymbol{x}})\right]^{-1} \tag{27}$$

following from the identity $\boldsymbol{x} = F_i(F_i^{-1}(\boldsymbol{x}))$. The computation of the inverse matrix in (27) is simpler than the evaluation of F_i^{-1}.

Further, the boundary integral over a side $\Gamma_{ij} \subset \bar{K}_i$ in the form b_h in (10) is computed with the aid of

$$\begin{aligned} &\int_{\Gamma_{ij}} \boldsymbol{H}(\boldsymbol{w}_h^+(\boldsymbol{x}, t), \boldsymbol{w}_h^-(\boldsymbol{x}, t), \boldsymbol{n}_{ij}) \cdot \boldsymbol{\varphi}_h(\boldsymbol{x}) \, \mathrm{d}S \\ &= \int_{\hat{\Gamma}} \boldsymbol{H}(\boldsymbol{w}_h^+(F_i(\hat{\boldsymbol{x}}), t), \boldsymbol{w}_h^-(F_i(\hat{\boldsymbol{x}}), t), \hat{\boldsymbol{n}}_{ij}(\hat{\boldsymbol{x}})) \cdot \hat{\boldsymbol{\varphi}}(\hat{\boldsymbol{x}}) \beta(\hat{\boldsymbol{x}}) \, \mathrm{d}\hat{S}, \end{aligned} \tag{28}$$

where $\hat{\Gamma}$ is the side of $\hat{K}$ corresponding to the curved side of $\bar{K}_i$ in the mapping F_i and $\boldsymbol{w}_h^{\pm}(\boldsymbol{x}, t) = \boldsymbol{w}_h^{\pm}(F_i(\hat{\boldsymbol{x}}), t)$. The function $\beta(\hat{\boldsymbol{x}})$ represents a boundary increase for boundary integral in a suitable parametrization $x_1 = x_1(s), x_2 = x_2(s)$:

$$\int_{\Gamma} u(x_1, x_2)\,\mathrm{d}S = \int_{s_1}^{s_2} u(x_1(s), x_2(s))\sqrt{(x_1'(s))^2 + (x_2'(s))^2}\,\mathrm{d}s = \tag{29}$$
$$= \int_{\hat{s}_1}^{\hat{s}_2} u(F_i^1(\hat{x}_1(\hat{s}), \hat{x}_2(\hat{s})), (F_i^2(\hat{x}_1(\hat{s}), \hat{x}_2(\hat{s})))\beta(\hat{x}_1(\hat{s}), \hat{x}_2(\hat{s}))\mathrm{d}\hat{s}.$$

Finally, the integrals over the reference triangle $\hat{K}$ and over the reference edge $\hat{\Gamma}$ in (25), (26), (28) are evaluated with the aid of (14) and (13), respectively. Such approach essentially improves the quality of the solution in a neighbourhood of curved parts of the boundary as is shown in Section 6, Figures 4 and 5.

6 Numerical examples

The first numerical example deals with transonic flow through the GAMM channel. The inlet Mach number = 0.67 produces a shock wave. In order to obtain a steady state solution, we apply the time stabilization method ($t \to \infty$).

We demonstrate the influence of the use of the bilinear mapping for triangles lying at the curved part of $\partial\Omega$ explained in Section 5. The computations were performed on a very coarse grid from Figure 3 having 784 triangles where such effect is better observed. Figures 4 and 5 show the distribution of the density in the computational domain and along the lower wall obtained by scheme (11) without and with the use of the bilinear mapping.

Figure 7 shows the distribution of the density in Ω and along the lower wall obtained with the aid of the bilinear mapping on refined mesh shown in Figure 6. This triangulation was refined by an anisotropic mesh adaptation technique from [7]. Here a very sharp capturing of the shock wave and the Zierep singularity is observed.

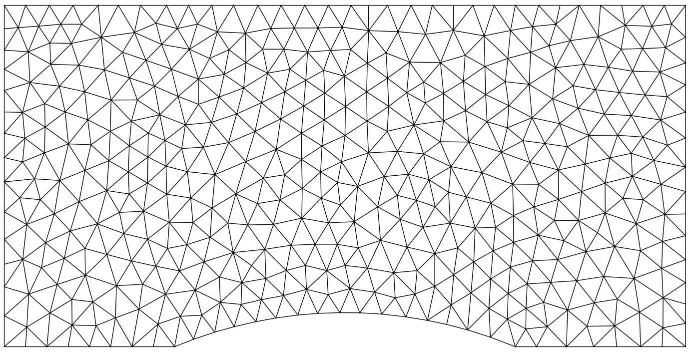

Fig. 3. Coarse triangular mesh (784 triangles)

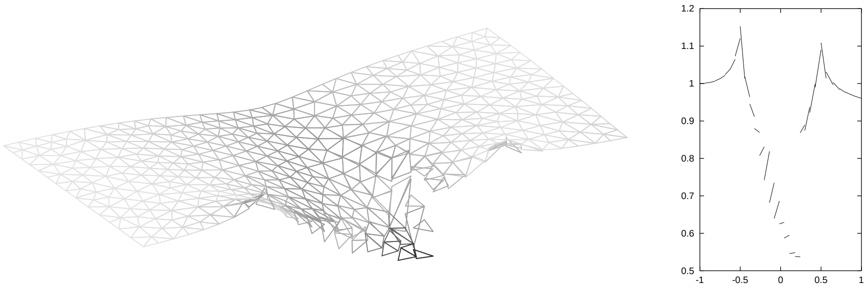

Fig. 4. Distribution of the density in the computational domain and along the lower wall without the use of the bilinear mapping at $\partial\Omega$

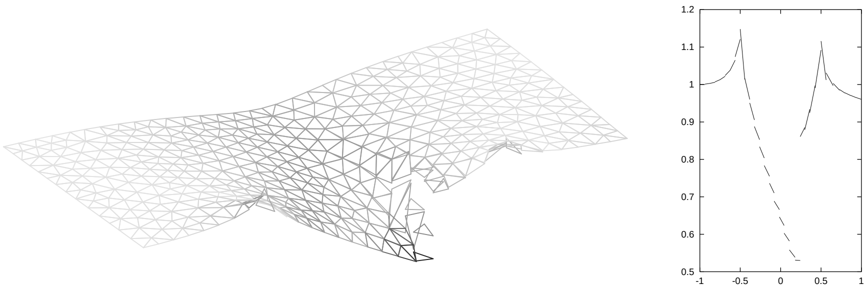

Fig. 5. Distribution of the density in the computational domain and along the lower wall with the use of the bilinear mapping for at $\partial\Omega$

The second example is concerned with the computation of inviscid compressible flow past the airfoil NACA0012 with far field Mach number = 0.8 and angle of attack = 1.25^o. To achieve a sharp capturing of shock wave, the anisotropic mesh adaptation method was applied. Figure 8 shows the used triangulation and computed Mach number isolines.

7 Error analysis for a model problem

In this section we are concerned with theoretical analysis of one version of the DG FE method with order limiting carried out with the aid of local averaging in the convection form and applied to a model nonlinear nonstationary convection-diffusion problem.

Let $\Omega \subset I\!R^2$ be a bounded polygonal domain and $T > 0$. We set $Q_T = \Omega \times (0, T)$ and by $\partial\Omega$ denote the boundary of Ω. We consider the following model *initial-boundary value problem*: Find $u : Q_T \to I\!R$ such that

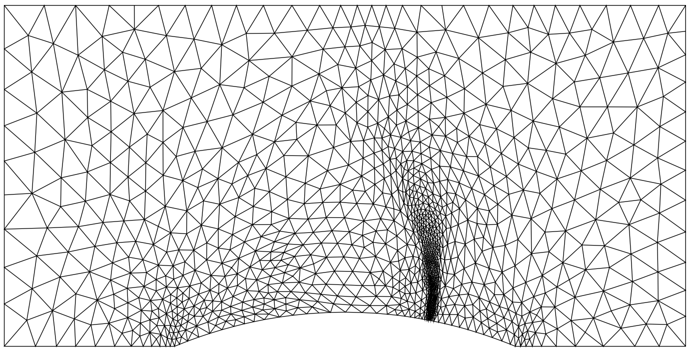

Fig. 6. Adapted triangular mesh (2131 triangles)

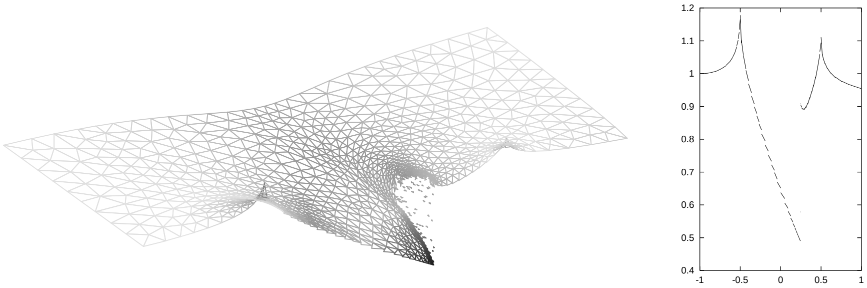

Fig. 7. Distribution of the density in the computational domain and along the lower wall with bilinear mapping on adapted mesh

$$\frac{\partial u}{\partial t} + \sum_{s=1}^{2} \frac{\partial f_s(u)}{\partial x_s} = \varepsilon \Delta u + g \quad \text{in } Q_T, \tag{30}$$

$$u|_{\partial\Omega\times(0,T)} = u_D, \tag{31}$$

$$u(x,0) = u^0(x), \quad x \in \Omega. \tag{32}$$

We suppose that $f_s \in C^1(\mathbb{R})$ and the data are sufficiently regular so that we can assume the existence of a *strong solution* u satisfying (30) – (32) pointwise:

$$u \in L^2(0,T;H^2(\Omega)), \partial u/\partial t \in L^2(0,T;H^1(\Omega)). \tag{33}$$

In order to discretize the above model problem, we introduce the following notation: $h_K = \mathrm{diam}(K)$, $h = \max_{K\in\mathcal{T}_h} h_K$, ρ_k = radius of the largest circle inscribed into K, $\boldsymbol{n}_{ij} = ((n_{ij})_1, (n_{ij})_2)$ = unit outer normal to ∂K_i on the side Γ_{ij}, $|\Gamma_{ij}|$=length of Γ_{ij}, $|K|$ = two-dimensional Lebesgue measure of $K \in \mathcal{T}_h$. For $v \in H^1(\Omega, \mathcal{T}_h)$ we define $v|_{\Gamma_{ij}}$ = the trace of $v|_{K_i}$ on $\Gamma_{ij}, v|_{\Gamma_{ji}}$ = the trace of $v|_{K_j}$on $\Gamma_{ji} = \Gamma_{ij}, \langle v\rangle_{\Gamma_{ij}} = \frac{1}{2}\left(v|_{\Gamma_{ij}} + v|_{\Gamma_{ji}}\right), \quad [v]_{\Gamma_{ij}} = v|_{\Gamma_{ij}} - v|_{\Gamma_{ji}}$.

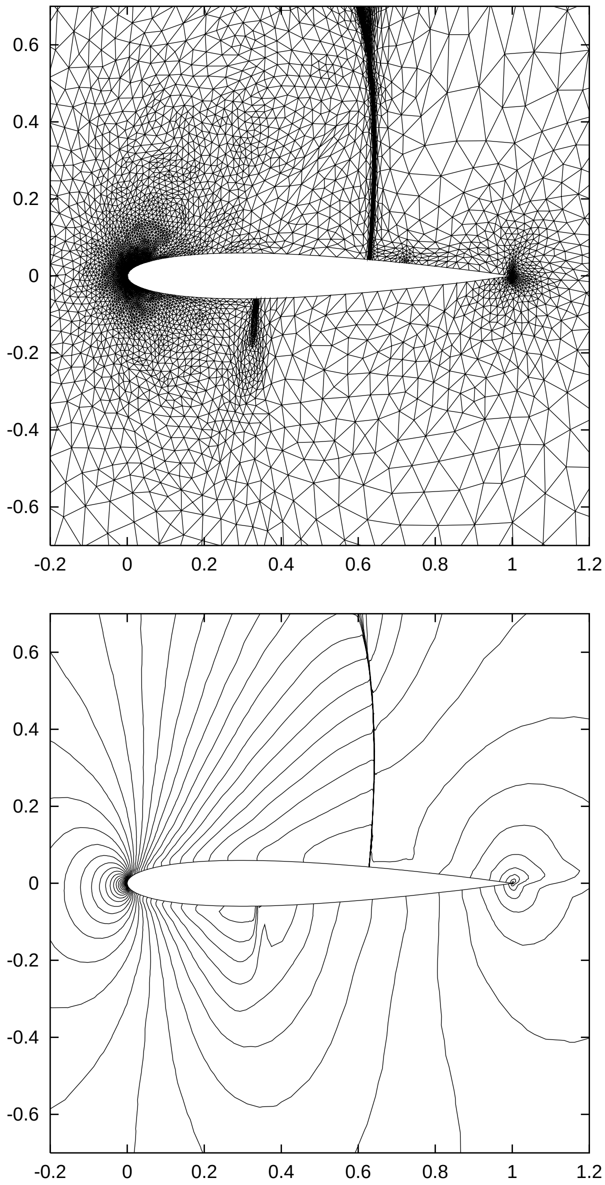

Fig. 8. Transonic flow around NACA0012: triangulation and the isolines of Mach number

For $u_h, v_h \in S_h$ we set

$$\begin{aligned} a_h(u_h, v_h) = {} & \varepsilon \sum_{i\in I} \int_{K_i} \nabla u_h \cdot \nabla v_h \,\mathrm{d}x \\ & -\varepsilon \sum_{i\in I} \sum_{\substack{j\in s(i)\\ j<i}} \int_{\Gamma_{ij}} \langle \nabla u_h \rangle \cdot \boldsymbol{n}_{ij} \, [v_h] \,\mathrm{d}S \\ & +\varepsilon \sum_{i\in I} \sum_{\substack{j\in s(i)\\ j<i}} \int_{\Gamma_{ij}} \langle \nabla v_h \rangle \cdot \boldsymbol{n}_{ij} \, [u_h] \,\mathrm{d}S \\ & -\varepsilon \sum_{i\in I} \sum_{j\in \gamma(i)} \int_{\Gamma_{ij}} \nabla u_h \cdot \boldsymbol{n}_{ij} \, v_h \,\mathrm{d}S \\ & +\varepsilon \sum_{i\in I} \sum_{j\in \gamma(i)} \int_{\Gamma_{ij}} \nabla v_h \cdot \boldsymbol{n}_{ij} \, u_h \,\mathrm{d}S \end{aligned} \tag{34}$$

(approximation of diffusion terms),

$$J_h^\sigma(u_h, v_h) = \sum_{i\in I} \sum_{j\in s(i)} \int_{\Gamma_{ij}} \sigma [u_h] \, [v_h] \,\mathrm{d}S + \sum_{i\in I} \sum_{j\in \gamma(i)} \int_{\Gamma_{ij}} \sigma \, u_h \, v_h \,\mathrm{d}S \tag{35}$$

(stabilization jump terms),

$$\begin{aligned} \ell_h(v_h)\,(t) = {} & \int_\Omega g(t) \, v_h \,\mathrm{d}x + \varepsilon \sum_{i\in I} \sum_{j\in \gamma(i)} \int_{\Gamma_{ij}} \nabla v_h \cdot \boldsymbol{n}_{ij} u_D(t) \,\mathrm{d}S \\ & +\varepsilon \sum_{i\in I} \sum_{j\in \gamma(i)} \int_{\Gamma_{ij}} \sigma \, u_D(t) \, v_h \,\mathrm{d}S, \end{aligned} \tag{36}$$

$$(\alpha, \beta) = \int_\Omega \alpha\beta \,\mathrm{d}x, \tag{37}$$

Here σ is a weight function such that $\sigma|_{\Gamma_{ij}} = 1/|\Gamma_{ij}|$.

Further, we define the approximate convection form with the aid of the local averaging procedure. We assume that $p = 1$ and for π_0 we denote the L^2-projection of functions $v \in L^2(\Omega)$ on the space $\mathcal{S}_h^{0,-1}(\Omega, \mathcal{T}_h)$ of piecewise constant functions: $\pi_0 v|_K = \int_K v \,\mathrm{d}x / |K|$ for $K \in \mathcal{T}_h$. Then, the convective terms are approximated by the form

$$\begin{aligned} b_h(u_h, v_h) = {} & \sum_{i\in I} \pi_0 v_h|_{K_i} \Big\{ \sum_{j\in s(i)} H\left(\pi_0 u_h|_{K_i}, \pi_0 u_h|_{K_j}, \boldsymbol{n}_{ij}\right) |\Gamma_{ij}| \\ & + \sum_{j\in\gamma(i)} H\left(\pi_0 u_h|_{K_i}, \pi_0 u_h|_{K_i}, \boldsymbol{n}_{ij}\right) |\Gamma_{ij}| \Big\}. \end{aligned} \tag{38}$$

As we see, the boundary values are realized in the form b_h by extrapolation.

Now, *the approximate solution* is defined as a function u_h satisfying the conditions

$$\text{a) } u_h \in C^1([0,T], S_h), \tag{39}$$

$$\text{b) } \left(\frac{\partial u_h(t)}{\partial t}, v_h\right) + b_h(u_h(t), v_h) + a_h(u_h(t), v_h) + \varepsilon J_h^\sigma(u_h(t), v_h) =$$
$$= \ell_h(v_h)(t), \qquad \forall\, v_h \in S_h \quad \forall\, t \in (0,T),$$

$$\text{c) } u_h(0) = u_h^0,$$

where u_h^0 is an S_h-approximation of u^0 (e. g., L^2-projection). We consider here the space discretization only, leaving time continuous. Of course, in practical computations also time discretization is carried out.

In order to derive *error estimates*, we consider the following *assumptions*: Let us consider a system $\{\mathcal{T}_h\}_{h\in(0,h_0)}$, $h_0 > 0$, of partitions of the domain Ω ($\mathcal{T}_h = \{K_i\}_{i\in I_h}$, $I_h \subset Z^+$, but for simplicity we write again I instead of I_h) and assume that it has the following properties:

(A1) There exists a constant $C_1 > 0$ such that

$$h_K/\rho_K \le C_1 \quad \forall\, K \in \mathcal{T}_h,\ \forall\, h \in (0, h_0). \tag{40}$$

(We say that the system $\{\mathcal{T}_h\}_{h\in(0,h_0)}$ is *shape regular*.)

(A2) There exists a constant C_2 such that

$$\operatorname{card} S(i) \le C_2 \quad \forall\, K_i \in \mathcal{T}_h,\ \forall\, h \in (0, h_0). \tag{41}$$

(The number of neighbours K_j of K_i is uniformly bounded.)

(A3) There exists a constant $C_3 > 0$ such that

$$h_{K_i} \le C_3 |\Gamma_{ij}|, \quad i \in I, j \in S(i), h \in (0, h_0). \tag{42}$$

(The length of faces between neighbouring elements does not degenerate.)

(A4) The numerical flux has the following properties:

1) $H(\alpha, \beta, \boldsymbol{n})$ is defined on $\mathbb{R}^2 \times B_1$, where $B_1 = \{\boldsymbol{n} \in \mathbb{R}^2; |\boldsymbol{n}| = 1\}$, is Lipschitz-continuous,
2) $H(\alpha, \beta, \boldsymbol{n})$ is *consistent*:
$$H(\alpha, \alpha, \boldsymbol{n}) = \sum_{s=1}^{2} f_s(\alpha)\, n_s, \quad \alpha \in \mathbb{R},\ \boldsymbol{n} = (n_1, n_2) \in B_1, \tag{43}$$
3) $H(\alpha, \beta, \boldsymbol{n})$ is *conservative*:
$$H(\alpha, \beta, \boldsymbol{n}) = -H(\beta, \alpha, -\boldsymbol{n}), \quad \alpha,\, \beta \in \mathbb{R},\ \boldsymbol{n} \in B_1. \tag{44}$$

7.1 Auxiliary estimates

Under the above assumptions, the following results can be established.

Lemma 7.1. (Multiplicative trace inequality) *There exists a constant $C_4 > 0$ independent of h, K such that*

$$\|v\|^2_{L^2(\partial K)} \le C_4 \left(\|v\|_{L^2(K)}\, |v|_{H^1(K)} + h_K^{-1} \|v\|^2_{L^2(K)} \right), \qquad (45)$$
$$K \in \mathcal{T}_h,\ v \in H^1(K),\ h \in (0, h_0).$$

Lemma 7.2. The following estimates hold:

$$\|\pi_0 v\|_{L^2(K)} \le \|v\|_{L^2(K)}, \quad K \in \mathcal{T}_h,\ v \in L^2(K), \qquad (46)$$
$$\|\pi_0 v\|_{L^2(\Omega)} \le \|v\|_{L^2(\Omega)}, \quad v \in L^2(\Omega), \qquad (47)$$
$$\|v - \pi_0 v\|_{L^2(K)} \le \frac{h_K}{\pi} |v|_{H^1(K)}, \quad K \in \mathcal{T}_h,\ v \in H^1(K), \qquad (48)$$
$$\|v - \pi_0 v\|_{L^2(\partial K)} \le C_5\, h_K^{1/2} |v|_{H^1(K)}, \quad K \in \mathcal{T}_h,\ v \in H^1(K), \qquad (49)$$

with a constant $C_5 > 0$ independent of $h \in (0, h_0)$ and K, v.

There exist a constant $C_6 > 0$ independent of $h \in (0, h_0)$ and v and a mapping $\Pi : H^1(\Omega, \mathcal{T}_h) \to S_h$ such that

$$\|\Pi v - v\|_{L^2(K)} \le C_6 h_K |v|_{H^1(K)}, \quad v \in H^1(K), \qquad (50)$$
$$\|\Pi v - v\|_{L^2(K)} \le C_6 h_K^2 |v|_{H^2(K)}, \quad v \in H^2(K),$$
$$|\Pi v - v|_{H^1(K)} \le C_6 h_K |v|_{H^2(K)}, \quad v \in H^2(K),$$
$$K \in \mathcal{T}_h,\ h \in (0, h_0),$$

$$\|\Pi v - v\|_{L^2(\Omega)} \le C_6 h |v|_{H^1(\Omega, \mathcal{T}_h)}, \quad v \in H^1(\Omega, \mathcal{T}_h), \qquad (51)$$
$$\|\Pi v - v\|_{L^2(\Omega)} \le C_6 h^2 |v|_{H^2(\Omega, \mathcal{T}_h)}, \quad v \in H^2(\Omega, \mathcal{T}_h),$$
$$|\Pi v - v|_{H^1(\Omega, \mathcal{T}_h)} \le C_6 h |v|_{H^2(\Omega, \mathcal{T}_h)}, \quad v \in H^2(\Omega, \mathcal{T}_h).$$

7.2 Properties of the form b_h

Lemma 7.3. The form b_h is Lipschitz continuous: There exists a constant $C_7 > 0$ such that

$$|b_h(u_h, v_h) - b_h(u, v_h)| \le \qquad (52)$$
$$\le C_7 \left(J_h^\sigma(v_h, v_h)^{1/2} + |v_h|_{H^1(\Omega, \mathcal{T}_h)} \right) \|u - u_h\|_{L^2(\Omega)},$$
$$u_h \in S_h,\ u \in L^2(\Omega),\ v_h \in S_h,\ h \in (0, h_0).$$

Moreover, b_h is consistent: There exists a constant $C_8 > 0$ such that

$$|b_h(u, v_h) - b(u, v_h)| \le \qquad (53)$$
$$\le C_8\, h |u|_{H^1(\Omega)} \left(J_h^\sigma(v_h, v_h)^{1/2} + |v_h|_{H^1(\Omega, \mathcal{T}_h)} \left(\Phi(\|u\|_{L^\infty(\Omega)}) + 1 \right) \right),$$
$$u \in H^1(\Omega) \cap L^\infty(\Omega),\ v_h \in S_h,\ h \in (0, h_0),$$

where we define, for $M \geq 0$,

$$\Phi(M) = \max_{\substack{\xi \in [-M,M] \\ s=1,\dots,d}} |f_s'(\xi)| \tag{54}$$

and

$$b(u, v_h) = \int_\Omega \sum_{s=1}^{2} \frac{\partial f_s(u)}{\partial x_s} v_h \mathrm{d}\boldsymbol{x} \tag{55}$$

is a weak form of the convection terms from the continuous problem.

7.3 Derivation of the error estimate

Let us assume that the exact solution satisfies conditions (33). Then it satisfies the relation

$$\left(\frac{\partial u}{\partial t}, v_h\right) + a_h(u, v_h) + \varepsilon J_h^\sigma(u, v_h) + b(u, v_h) = \ell(v_h) \quad \forall v_h \in S_h. \tag{56}$$

We set

$$M = \|u\|_{L^\infty(Q_T)}. \tag{57}$$

and

$$\xi = u_h - \Pi u, \quad \eta = \Pi u - u. \tag{58}$$

Then

$$u_h - u = \xi + \eta, \quad \xi(t) \in S_h, \quad \eta(t) \in H^2(\Omega, \mathcal{T}_h), \quad t \in [0, T]. \tag{59}$$

From the numerical scheme (39), where we write b_h instead of $\tilde{b}_h$, and identity (56), it is possible to derive the relation

$$\begin{aligned} &\left(\frac{\partial \xi}{\partial t}, \xi\right) + a_h(\xi, \xi) + \varepsilon J_h^\sigma(\xi, \xi) \\ &= b(u, \xi) - b_h(u_h, \xi) - \left(\frac{\partial \eta}{\partial t}, \xi\right) - a_h(\eta, \xi) - \varepsilon J_h^\sigma(\eta, \xi). \end{aligned} \tag{60}$$

In the sequel, we estimate the individual terms on the right-hand side of (60) and get the following results:.

Lemma 7.4. It holds:

$$\frac{1}{2}\left(\frac{\partial \xi}{\partial t}, \xi\right) = \frac{\mathrm{d}}{\mathrm{d}t}\|\xi\|^2_{L^2(\Omega)}, \tag{61}$$

$$\left|\left(\frac{\partial \eta}{\partial t}, \xi\right)\right| \leq \left\|\frac{\partial \eta}{\partial t}\right\|_{L^2(\Omega)} \|\xi\|_{L^2(\Omega)}, \tag{62}$$

$$J_h^\sigma(\eta, \xi) \leq \left(J_h^\sigma(\eta, \eta)\right)^{1/2} \left(J_h^\sigma(\xi, \xi)\right)^{1/2}, \tag{63}$$

$$
\begin{aligned}
\|\eta\|_{L^2(\Omega)} &\le C_9 h |u|_{H^1(\Omega)}, \\
\|\eta\|_{L^2(\Omega)} &\le C_9 h^2 |u|_{H^2(\Omega)}, \\
|\eta|_{H^1(\Omega,\mathcal{T}_h)} &\le C_9 h |u|_{H^2(\Omega)}, \\
\left\|\frac{\partial \eta}{\partial t}\right\|_{L^2(\Omega)} &\le C_9 h \left|\frac{\partial u}{\partial t}\right|_{H^1(\Omega)}, \quad h \in (0, h_0),
\end{aligned}
\tag{64}
$$

where $C_9 > 0$ is a constant independent of u and h.

Lemma 7.5. We have

$$
\begin{aligned}
|b(u,\xi) - b_h(u_h,\xi)| \le C_{10} &\left(J_h^\sigma(\xi,\xi)^{1/2} + |\xi|_{H^1(\Omega,\mathcal{T}_h)} \right) \\
&\times \left(\|\xi\|_{L^2(\Omega)} + h^2 |u|_{H^2(\Omega)} + h|u|_{H^1(\Omega)} \right), \ h \in (0,h_0),
\end{aligned}
\tag{65}
$$

where $C_{10} > 0$ is a constant dependent on $M = \|u\|_{L^\infty(Q_T)}$ but independent of h and ξ. Moreover, there exists a constant $C_{11} > 0$ independent of u, h, ξ, ε such that

$$
|a_h(\eta,\xi)| \le C_{11} \varepsilon h |u|_{H^2(\Omega)} \left(J_h^\sigma(\xi,\xi)^{1/2} + |\xi|_{H^1(\Omega,\mathcal{T}_h)} \right), \quad h \in (0,h_0). \tag{66}
$$

The last step in the proof of error estimates is the application of Gronwall's lemma. This yields the *main result*.

Theorem 7.1. Let assumptions (A1) – (A4) be satisfied. Let u be the exact strong solution of problem (30) – (32) satisfying (33) and let u_h be the approximate solution defined by scheme (39). Then the error $e_h = u_h - u$ satisfies the estimate

$$
\begin{aligned}
&\sup_{t\in[0,T]} \|e_h(t)\|^2_{L^2(\Omega)} + \varepsilon \int_0^T \left(|e_h(\vartheta)|^2_{H^1(\Omega,\mathcal{T}_h)} + J_h^\sigma(e_h(\vartheta), e_h(\vartheta)) \right) \mathrm{d}\vartheta \\
&\le C\, h^2, \quad h \in (0,h_0).
\end{aligned}
\tag{67}
$$

with a constant $C > 0$ independent of h.

All proofs are rather technical. The detailed theory was worked out in cooperation with C. Schwab and will appear in a separate paper [8].

As we see from (67), the analyzed scheme obtained by the modification of the DG FE method is of the first order only. This is caused by the fact that the order limiting based on the local averaging procedure is applied on all elements. It is necessary to mention that the constant C from the above estimate depends on $\varepsilon \to 0$ in a very pessimistic way: $C \approx \exp(c/\varepsilon)$ (c is a constant independent of h and ε). This is caused by the application of Young's inequality and Gronwall's lemma. A uniform estimate for $\varepsilon \to 0$ remains open.

8 Conclusion

We present the application of the discontinuous Galerkin method for the numerical solution of the system of the compressible Euler equations. The piecewise linear approximation on triangular grids is implemented. Numerical examples show that in order to avoid spurious oscillations near shock waves, a limiting based on the control of interelement jumps of density and the decrease of the polynomial degree to zero has to be applied. Moreover, in order to obtain a good solution in the vicinity of curved boundaries, it is necessary to use isoparametric finite elements.

The extension to viscous compressible high speed flow (the solution of the compressible Navier–Stokes equations) and implementation of higher order approximations with suitable limiting in the vicinity of shock waves will be the subject matter of forthcoming papers. The theoretical analysis of presented schemes is quite incomplete and a number of open questions should be answered.

Acknowledgment This research is supported under the Grant No. 201/02/0684 and No. 201/00/D116 of the Czech Grant Agency and the Grant No. MSM 113200007.

References

1. P. Angot, V. Dolejší, M. Feistauer, and J. Felcman. Analysis of a combined barycentric finite volume – nonconforming finite element method for nonlinear convection – diffusion problem. *Applications of Mathematics*, 43(4):263–310, 1998.
2. F. Bassi and S. Rebay. High-order accurate discontinuous finite element solution of the 2D Euler equations. *J. Comput. Phys.* 138:251-285, 1997.
3. F. Bassi and S. Rebay. A high-order accurate discontinuous finite element method for the numerical solution of the compressible Navier-Stokes equations. *J. Comput. Phys.* 131:267-279, 1997.
4. F. Brezzi, G. Manzini, D. Marini, P. Pietra and A. Russo: Discontinuous Galerkin approximations for elliptic problems. *Numer. Methods Partial Differential Eq.* 16:365-378, 2000.
5. B. Cockburn. Discontinuous Galerkin methods for convection dominated problems. In T. J. Barth and H. Deconinck, editors, *High–Order Methods for Computational Physics*, number 9 in Lecture Notes in Computational Science and Engineering, pages 69–224. Springer, Berlin, 1999.
6. B. Cockburn, G. E. Karniadakis, and C.-W. Shu (eds.). Discontinuous Galerkin methods. In *Lecture Notes in Computational Science and Engineering 11*. Springer, Berlin, 2000.
7. V. Dolejší. Anisotropic mesh adaptation for finite volume and finite element methods on triangular meshes. *Computing and Visualization in Science*, 1(3):165–178, 1998.

8. V. Dolejší, M. Feistauer, and C. Schwab. A finite volume discontinuous Galerkin scheme for nonlinear convection-diffusion problems. *Calcolo*, (to appear). also Preprint ETH Zurich, January 2001.
9. V. Dolejší, M. Feistauer, and C. Schwab. On some aspects of the discontinuous Galerkin finite element method for conservation laws. *Mathematics and Computers in Simulation*, (submitted).
10. M. Feistauer. *Mathematical Methods in Fluid Dynamics.* Longman Scientific & Technical, Harlow, 1993.
11. M. Feistauer and J. Felcman. Convection-Diffusion Problems and Compressible Navier–Stokes Equations. In J. R. Whitemen, editor, *The Mathematics of Finite Elements and Applications*, pages 175–194. John Wiley & Sons, 1996.
12. M. Feistauer, J. Felcman, and V. Dolejší. Numerical simulation of compresssible viscous flow through cascades of profiles. *ZAMM*, 76:297–300, 1996.
13. M. Feistauer, J. Felcman, and M. Lukáčová. Combined finite elements–finite volume solution of compressible flow. *J. Comput. Appl. Math.*, 63:179–199, 1995.
14. M. Feistauer, J. Felcman, and M. Lukáčová. On the convergence of a combined finite volume – finite element method for nonlinear convection – diffusion problems. *Numer. Methods for PDE's*, 13:163–190, 1997.
15. M. Feistauer, J. Felcman, M. Lukáčová, and G. Warnecke. Error estimates of a combined finite volume – finite element method for nonlinear convection – diffusion problems. *SIAM J. Numer. Anal.*, 36:1528–1548, 1999.
16. J. Felcman. On a 3D adaptation for compressible flow. In *Proceedings of the conf. "Finite Element Methods for Three-Dimensional Problems"*, page (to appear), June 27 – July 1, 2000.
17. J. Felcman and P. Šolín. On the construction of the Osher–Solomon scheme for 3D Euler equations. *East–West J. Numer. Math*, 6:1, 1998.
18. R. Hartmann and P. Houston. Adaptive discontinuous Galerkin finite element methods for nonlinear conservation laws. Technical Report Preprint 2001–20, SFB 359, Universität Heidelberg, 2001.
19. S. Osher and F. Solomon. Upwind difference schemes for hyperbolic systems of conservation laws. *Math. Comp.*, 38:339–374, 1982.
20. P. Houston, C. Schwab and E. Süli: Discontinuous $hp-$finite element method for advection-diffusion problems. Research Report No. 2000-07, SAM ETH Zürich, 2000.
21. S. P. Spekreijse: Multigrid Solution of the Steady Euler Equations. Centrum voor Wiskunde en Informatica, Amsterdam, 1987.

List of preprints released in this series

[MATH-kma-2002/1] W.Desch, E. Fasanga, J.Milota: *Unbounded observers and Riccati operators in nonreflexive spaces* (07.01.2002)